JOURNAL OF AIRCRAFT
Vol. 43, No. 4, July–August 2006

Investigating Correlations Between Reynolds-Averaged Flowfields and Noise for Forced Mixed Jets

C. W. Wright,* G. A. Blaisdell,† and A. S. Lyrintzis‡
Purdue University, West Lafayette, Indiana 47907

Jet engine manufacturers have known for some time that mixer design has a strong influence on jet noise, but the correlation between the two is unclear. The Reynolds-averaged Navier Stokes (RANS) computed steady-state flowfields of several mixers for which the far-field noise characteristics are known are analyzed. Three mixers with different lobe penetration heights are examined. The WIND computational fluid dynamics (CFD) code is used and compared with results from recent experiments conducted at the NASA John H. Glenn Research Center at Lewis Field. The Menter shear stress transport turbulence model and computational meshes of 1.9 million grid points are used for the comparisons. The turbulent kinetic energy profiles predicted by CFD are in good qualitative agreement with experimental data. Inferences are also made as to what correlations can be drawn between the RANS computed flowfield and the experimentally determined far-field noise and how this information may be used as an aid in mixer design.

Nomenclature

k = turbulent kinetic energy
y = distance from a grid point of interest to a wall
ε = turbulent kinetic energy dissipation rate
ν_w = kinematic viscosity on a wall
ρ_w = density on a wall
τ_w = viscous shear stress on a wall
ω = dissipation rate per unit turbulent knetic energy

I. Introduction

A. Motivation and Background

WITH the introduction of increasingly strict aircraft noise regulations, jet engine noise has become a very important issue. To remain competitive, jet engine manufacturers have spent millions of dollars to reduce their far-field noise emissions. Government agencies also continue their research toward reducing jet engine noise in an effort to improve the quality of life in communities that lie adjacent to large airports. Because details of the mechanism of this turbulent noise generation are not well understood, this task is made more difficult, especially when internal mixers are involved.

Although there are computational techniques to predict noise from jets using first principles, these techniques and the computational power required to implement them have not yet been fully developed as useful design tools. The most computationally intensive of these techniques is direct numerical simulation (DNS).[1] With DNS, one computes the flowfield for all relevant scales with no turbulence modeling. To maintain stability and to capture high-frequency noise, the grid must be very fine. (The higher the Reynolds number the smaller the small-scale turbulent eddies are.) To keep the number of grid points from becoming excessive, DNS must be run at low Reynolds numbers. At the present time, DNS is only useful as a research tool. This is because the extremely low Reynolds numbers do not reflect realistic noise problems.

Received 4 August 2004; revision received 14 September 2005; accepted for publication 28 September 2005.

*Graduate Research Assistant, School of Aeronautics and Astronautics. Student Member AIAA.
†Associate Professor, School of Aeronautics and Astronautics. Senior Member AIAA.
‡Professor, School of Aeronautics and Astronautics. Associate Fellow AIAA.

Large-eddy simulation (LES) is another computational technique that has been applied to the jet noise problem. This technique allows higher Reynolds number flows than DNS. In LES, large eddies are computed directly, whereas small eddies are modeled by using a subgrid-scale model or by simply filtering the flow. The main advantage of LES is that simulating practical Reynolds number flows is feasible, although very expensive. Unfortunately, including nozzle geometry in the mesh increases this cost to impractical levels, and because there is currently no practical subgrid-scale noise model, all of the unresolved frequencies are lost.[2,3]

In contrast to DNS and LES, in which realistic computations that include nozzle geometry are not practical, Reynolds-averaged Navier–Stokes (RANS) computations can be done for almost any geometry and at realistic Reynolds numbers. Unlike DNS and LES, which compute some or all of the turbulence, RANS only computes the average flowfield and must account for the effects of the turbulence through modeling. Because the turbulent fluctuations are not known, an empirical or semi-empirical technique must be used to predict the noise. Whereas most empirical and semi-empirical techniques are easily applied, they have not been particularly successful in predicting noise for forced mixed jets. Forced mixed jets are very common and typically incorporate periodic (nonaxisymmetric) internal geometries to induce mixing. The most common semi-empirical technique is Mani Gliebe Balsa (MGB),[4] which is based on Lighthill's acoustic analogy[5] and utilizes RANS data. Barber and Chiappetta[6] attempted to predict noise from mixed jets using this technique. They obtained favorable results for axisymmetrics jets, but were less successful with nonaxisymmetric lobed (Fig. 1) mixers. They found that MGB can predict the trend between lobed and nonlobed mixers, but it breaks down when comparing lobed mixers of different designs. They attributed this as being "largely due to the inability of the circumferential averaging procedure to represent the 3-D problem."[6]

Another technique, recently developed by Fisher et al.[7,8] for the prediction of noise from coaxial jets, is the four-source method. This method treats mixed coaxial jets as four distinct sources that are characterized as individual single-stream jets. Single-stream jet noise data of the appropriate characteristic velocity and length scales is then combined to predict the noise of the coaxial mixed jet. Although this technique is only for coaxial jets, research is being conducted by Tester et al.[9] and Tester and Fisher[10] to extend this method for use with lobed mixers. Similar work based on the four-source method by Garrison et al.[11–13] involves trying to develop a two-source semi-empirical model that can predict the noise from forced mixed jets.

More general work on noise reduction for forced jets has been conducted by several researchers, as well. Pinker and Strange[14]

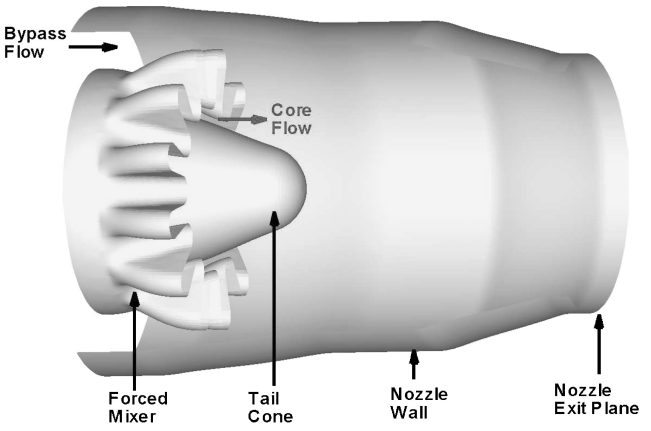

Fig. 1 Schematic of internally mixed engine nozzle with lobed mixer.

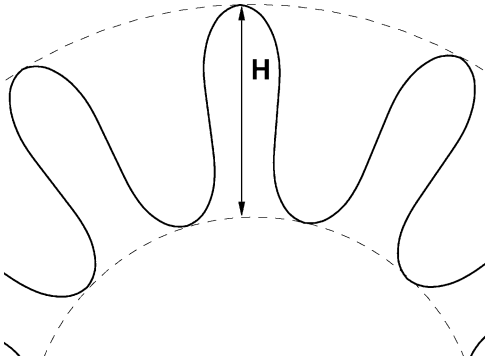

Fig. 2 Definition of penetration height *H*.

found that "increased mixing efficiency (unless 100%) does not necessarily result in improved noise performance." They noted that there is a high-frequency noise penalty associated with forced mixing. Saiyed et al.[15] used experimental acoustic data to support the idea of an external "residual mixing region" as the primary source of high-frequency mixing noise. Saiyed et al. defined this region as an area just downstream of the nozzle exit where the effects of the forced mixing are still strong.

B. Objectives

The far-field noise emitted from internally mixed turbofan engines (Fig. 1) as used on regional jet aircraft is quite sensitive to the flow mixer geometry. The goal of our work is to correlate some RANS computable flowfield characteristics to far-field noise levels for a relatively broad class of engines (internally mixed turbofans with lobed mixers). The scope of this work is limited to a single model of internally mixed regional jet engine, and the variable under control is the lobed mixer penetration height as defined Fig. 2. The primary purpose of lobed mixers is to increase the thrust and efficiency of internally mixed turbofans by creating a more uniform flow at the nozzle exit, but they also have a significant effect on the far-field noise. To determine a useful correlation using RANS, two things must be true. The noise must be a sufficiently strong function of some identifiable averaged flowfield quantity or characteristic, and the averaged flowfield must be computable with sufficient accuracy and efficiency to produce the applicable data. An earlier version of this work is also available.[16]

II. Development of the RANS Solutions

A. Selection of the Turbulence Model

The WIND CFD package was selected for use in this research. WIND[17] was developed by the NPARC Alliance, a partnership between the NASA John H. Glenn Research Center (GRC) and the U.S. Air Force Arnold Engineering Development Center (AEDC) in close association with The Boeing Company. Its default solution scheme is second-order upwind. The one-equation Spalart–Allmaras turbulence model[18] and the two-equation Menter shear stress transport (SST) turbulence model[19] are both available in this software package. These two models are the current state of the art for practical aerospace engineering applications, and they were both considered for use in this research. WIND also has the ability to coarsen or sequence the grid to accelerate the convergence.

The Spalart–Allmaras model is a one-equation model that was developed as a cost-effective way to solve aerodynamic flows with airfoils as the primary focus. The fact that it was designed with such a narrow focus would suggest that the Spalart–Allmaras model may not be ideal for more general flows; this, however, cannot be assumed.

One aspect of the Menter SST model is that it is a two-equation model that is a combination of the k–ε and k–ω models, where the k–ω model is implemented near solid walls and the k–ε model is implemented away from solid walls. The k–ω model works well for solid wall boundary layers, whereas using the k–ε model away from solid walls overcomes the k–ω model's sensitivity to freestream boundary conditions.

After several runs were completed with each turbulence model, it was found that Menter's SST model had slightly better agreement with experiment when comparing the axial velocity contours.[16] Menter's model also computes turbulent kinetic energy (which is available from experiments for comparison), whereas the Spalart–Allmaras model does not. Because of these factors, we chose the Menter SST model for use in this research.

B. Grid Dependence

Before a great deal of time is spent studying any solution, it is a good idea to determine the degree of grid dependence. Because of the high cost of increasing the grid resolution, it is not uncommon for large, practical applications to have some degree of grid dependence. It is often not practical to refine a grid to the point where the solution does not change noticeably with further refinement. It is, however, always a good idea to compare solutions of different grid refinement to determine some measure of this dependence.

In the early stages of this project, two different meshes were used. Both of these meshes extended 20.71 nozzle radii in the radial direction and 16.77 nozzle radii downstream of the nozzle exit. The freestream region of the grid extended 5.78 nozzle radii upstream of the nozzle exit plane, and the region inside the nozzle extended 3.93 nozzle radii upstream of the nozzle exit plane. These meshes modeled the high-penetration mixer and were run at the highest power setting. (See Sec. III for mixer and power setting details.) The first mesh had 800,000 grid points over 8 zones and was clearly inadequate for resolving the boundary and free shear layers. The second mesh consisted of 1.9 million grid points with 16 zones arranged as shown in Fig. 3 where the inflow boundaries are in the lower left corner, the outflow boundaries are to the right, and the two large zones at the top are primarily in the far-field/freestream region. This mesh had 10 times the solid wall grid resolution of the first mesh. A third mesh of approximately 8 million grid points and 16 zones was then created by increasing the number of grid points in the 1.9 million point grid by a factor of at least 1.5 in all three curvilinear directions. This was done to investigate the issue of grid dependence by comparing the new 8 million point solution to that of the 1.9 million point grid. All of these grids are pie shaped in cross section to take advantage of symmetry.

When Figs. 4 and 5, which show vorticity contours for the 1.9 million point grid, are compared to Figs. 6 and 7 for the 8 million point grid, the difference between the two solutions is not significant. This is further demonstrated in Fig. 8 by plotting the vorticity magnitude at the nozzle exit along a radial line centered in the the grid. In Fig. 8, we see that with the exception of a peak near the centerline the main features of the vorticity are captured with the 1.9 million point grid. The turnaround time, however, increased to approximately five days for the 8 million point grid as opposed to approximately 15–20 h for the 1.9 million point grid. Refining the mesh to the best possible solution is clearly not practical because we want to compute several lobed mixer flowfields at various operating

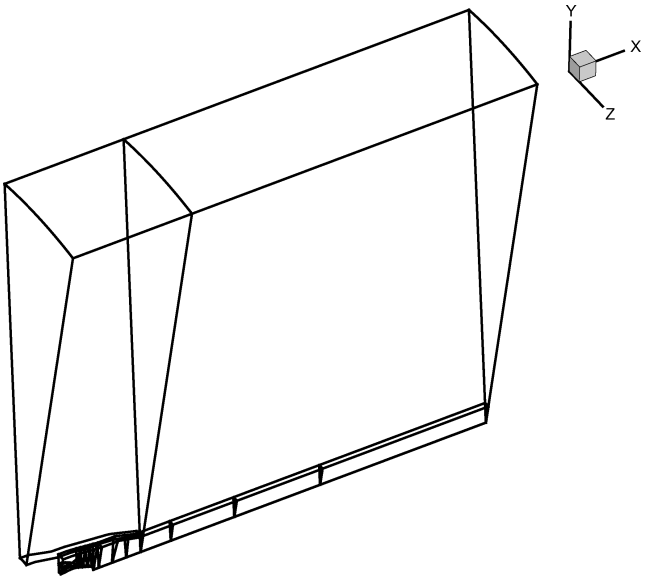

Fig. 3 Arrangement of 16 zones.

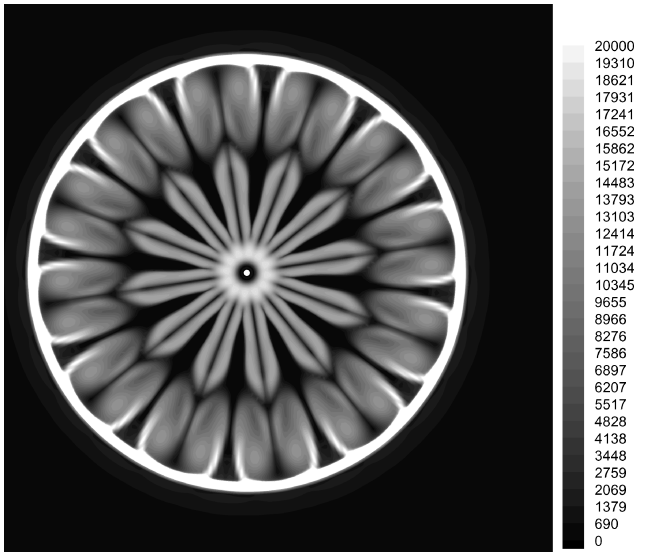

Fig. 4 Vorticity magnitude for WIND solution at 0.1 nozzle diameters downstream of nozzle exit; 1.9 million grid point solution.

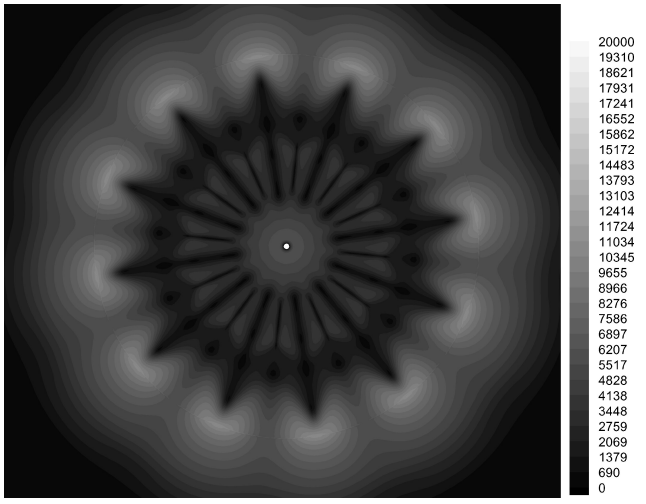

Fig. 5 Vorticity magnitude for the WIND solution at 2.0 nozzle diameters downstream of nozzle exit; 1.9 million grid point solution.

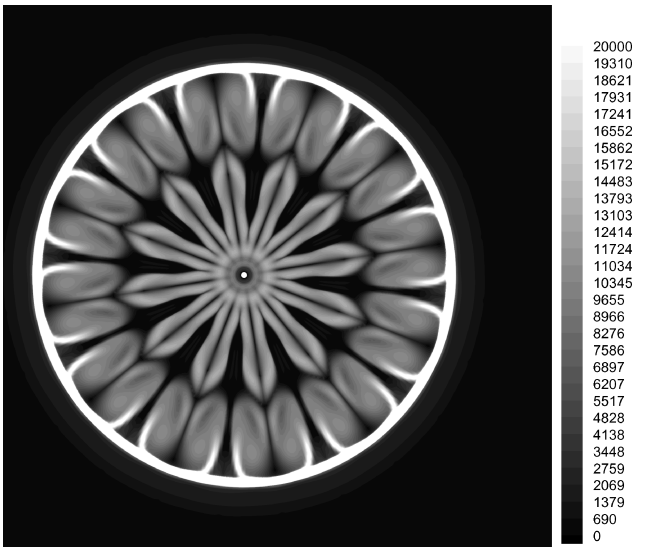

Fig. 6 Vorticity magnitude for the WIND solution at 0.1 nozzle diameters downstream of nozzle exit; 8 million grid point solution.

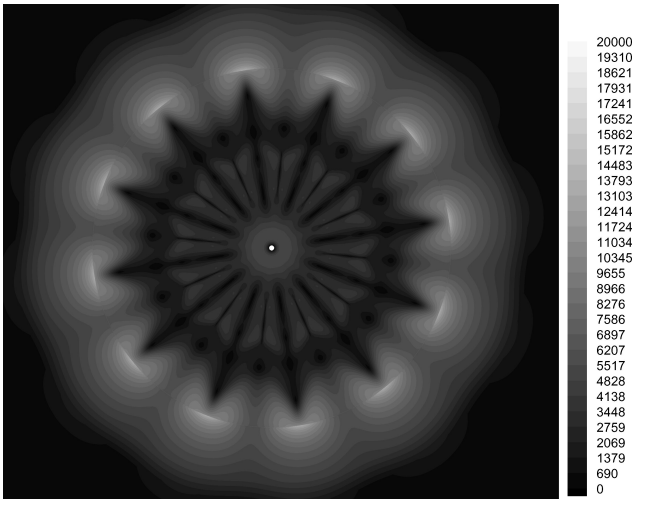

Fig. 7 Vorticity magnitude for the WIND solution at 2.0 nozzle diameters downstream of nozzle exit; 8 million grid point solution.

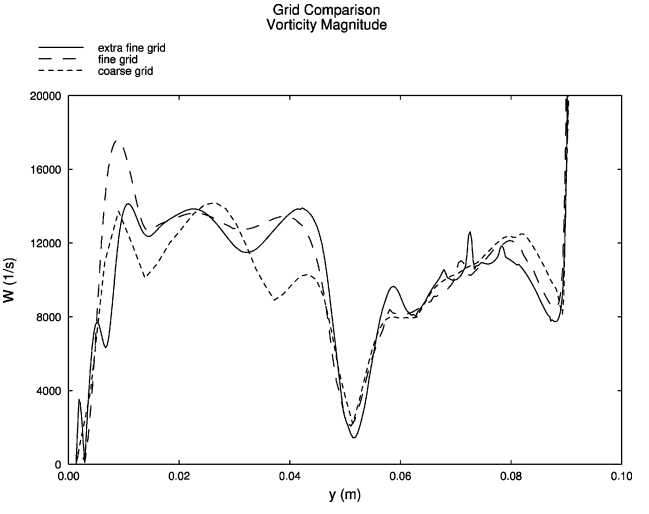

Fig. 8 Vorticity magnitude at the nozzle exit plane along a centered radial line (running from the jet axis to the nozzle wall): ——, 8 million point grid; — —, 1.9 million point grid; - - - -, 800,000 point grid.

conditions. When the immense increase in cost for very little gain is considered, the degree of grid dependence was deemed reasonable and the 1.9 million point mesh was chosen for the subsequent runs.

C. Boundary-Layer Grid Resolution

Boundary-layer resolution was also studied. A good measure of this resolution is the y^+ value at the first point off of a viscous wall. Distance y^+ is defined as follows:

$$y^+ = (y/\nu_w)\sqrt{\tau_w/\rho_w} \tag{1}$$

where y is the distance from the grid point of interest to the wall. White–Christoph wall functions have been used on all of the solutions, and the maximum recommended y^+ is 100 (see Ref. 17).

It was found that the y^+ values (as calculated by the WIND postprocessor) at the first point off the wall were less than 100 in most areas. There were, however, several regions where the y^+ was on the order of 200 and also a region on the lobed mixer wall where y^+ approached 1000. These values are high; however, the areas where these high values occurred consisted of a relatively small portion of the lobed mixer and nozzle wall surfaces. Also note that the WIND postprocessor defines y^+ based on the distance from the wall along the normal grid line, which is the grid line that intersects the wall at the point of interest. This works well if the normal grid line intersects the wall at nearly 90 deg, but will give a high y^+ value if the line intersects the wall at a sharp angle. On inspection it was found that sharp angles were occurring within the area of extremely high y^+ on the mixer wall. The WIND postprocessor calculated the peak y^+ at the first point off the wall as having a value of 978. However, the actual value if computed perpendicular to the wall is 156. Because of this normal-grid-line, effect and because all of the regions of high y^+ were small, the grid was determined to be adequately resolved in the boundary layers. The sensitivity of the flowfield to the mixer boundary layers was also evaluated by switching to an inviscid wall boundary condition on the lobe mixer surfaces for a single solution run. The resulting solution was qualitatively very similar to the viscous walled solution. This suggests that the flowfield is not extremely sensitive to the boundary layer and that small irregularities should have little effect on the overall solution.

III. Mixer Geometries and Effects on Noise

This section explains the selection and evaluation of the experimental acoustic data used in this project. The goal was to identify interesting trends that might have some correlation to the CFD results. In Sec. IV, the CFD flowfields are analyzed and compared to this section's acoustic evaluations.

Four different mixers (three lobed and one confluent) were selected for this project. For each of these geometries, there are three different power settings that were evaluated. The core and bypass absolute pressure ratios for these power settings are defined as total pressure divided by total ambient pressure and are given in Table 1. The flows all have Reynolds numbers ranging from about 8.9×10^5 for the low-power setting to about 1.2×10^6 for the high-power setting based on conditions at the nozzle exit jet centerline.

All of the raw noise data were taken at the NASA GRC Aero-Acoustic Propulsion Laboratory (AAPL) facility and have been corrected to a 50-ft (15.24 m) radius polar arc assuming an acoustic standard day: 70% relative humidity, 98.595 kPa, and 298.3 K (Ref. 20). The acoustic plots were created from this raw data by the authors. The variation in mixer geometry was limited to a single parameter, the mixer penetration height as defined in Fig. 2. The four different geometries, referred to as high penetration, medium penetration, low penetration, and confluent (no penetration), exhibited significant variation in their acoustic performance. The high-, medium-, (or mid-), and low-penetration mixers had nondimensional penetrations (normalized by the diameter of the duct at the mixer exit plane) of 0.172, 0.150, and 0.144, respectively. The area ratio (fan/core) is 2.637 for all mixers.

Table 1 Absolute temperature and pressure ratios for the three power settings

Setting	Core temperature ratio	Bypass temperature ratio	Core pressure ratio	Bypass pressure ratio
Low	2.80	1.20	1.39	1.44
Medium	3.13	1.20	1.54	1.61
High	3.34	1.20	1.74	1.82

A. Overall Sound Pressure Level Observations

In general, increased mixer penetration causes increased mixing, and a well-mixed jet is expected to make less noise than a poorly mixed jet. This reduction in noise is due to the flow cross section being more uniform and, therefore, lower in peak velocity for the well mixed flow.[21] This expected trend is confirmed by experiment for angles of above 130 deg (measured with 0 deg as the upstream axis and 180 deg as pointing downstream, as shown in Fig. 9), but is reversed below this angle as demonstrated by the overall sound pressure levels (OASPL) in Figs. 9–11 for the three power settings, respectively. This reversal is a well-observed phenomenon that is commonly attributed to additional noise sources associated with the mixing mechanism.[21] It seems that any gains made in reducing the noise in the high downstream angles and the lower frequencies (with frequency effects to be discussed later) are countered by some gain in noise for the upstream angles and the higher frequencies.

Figures 9–11 show the experimental OASPL values for the low; medium; and high-power settings, respectively. For the high- and middle-power settings, the OASPL of the high-penetration mixer are of similar magnitude to those of the medium-penetration mixer for angles of less than 120 deg. There is, however, a more significant decrease in the noise at angles above 120 deg for the high-penetration

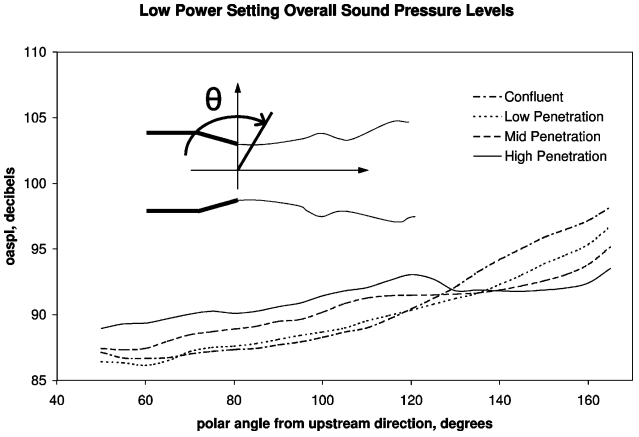

Fig. 9 OASPL for lowest power setting (raw data obtained from Bridges and Wernet[24]).

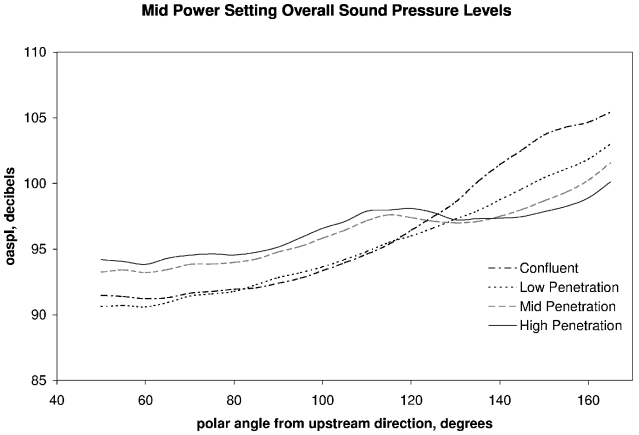

Fig. 10 OASPL for middle-power setting (raw data obtained from Bridges and Wernet[24]).

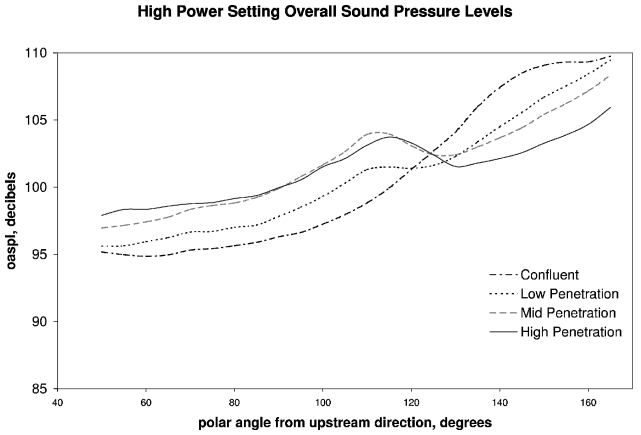

Fig. 11 OASPL for highest power setting (raw data obtained from Bridges and Wernet[24]).

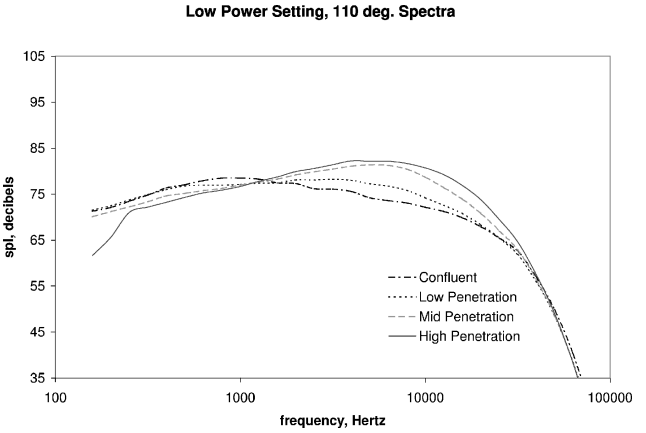

Fig. 12 Sound pressure spectra at 110 deg for lowest power setting (raw data obtained from Bridges and Wernet[24]).

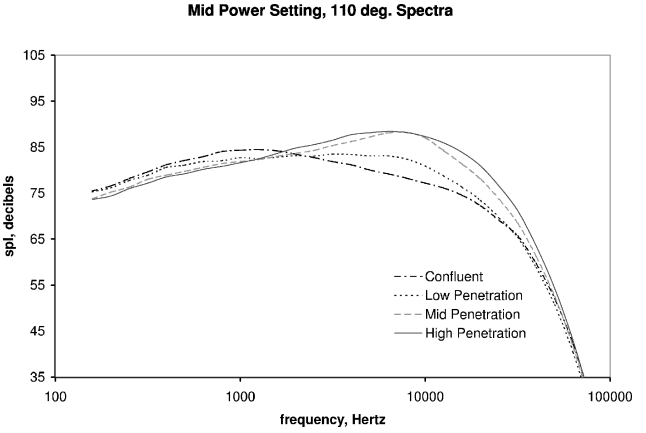

Fig. 13 Sound pressure spectra at 110 deg for middle-power setting (raw data obtained from Bridges and Wernet[24]).

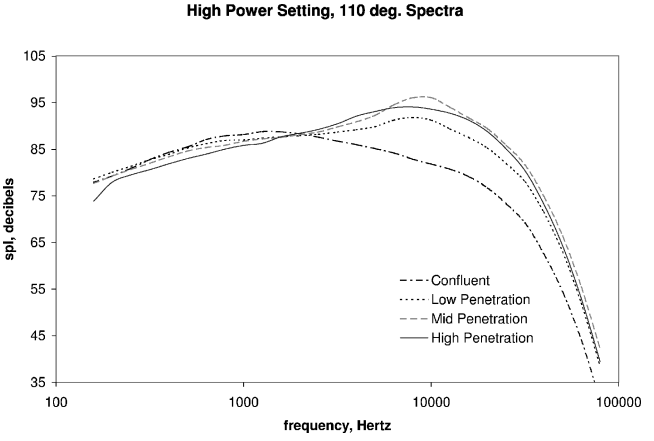

Fig. 14 Sound pressure spectra at 110 deg for highest power setting (raw data obtained from Bridges and Wernet[24]).

cases. It appears that the level of mixing noise (sideline and low angles) is similar for both the medium- and high-penetration mixers at these power settings. The additional mixing of the high-penetration case decreases the downstream jet noise with little penalty at upstream angles, except at the low-power setting. At the highest power setting, there is also a distinct peak at 110 deg for the midpenetration case. At this peak, the overall sound pressure of the midpenetration mixer is significantly higher than that of the high-penetration case. This local peak also exists for the midpenetration mixer at the middle-power setting, but it is much less pronounced and does not exceed the noise level of the high-penetration mixer.

Another observation is that whereas both the magnitude and shape of the OASPL curves change for different power settings, the low-penetration and midpenetration curves are always contoured very similarly (at like power settings) for angles of less than 110 deg. Although not conclusive, this at least suggests that the physics of the sound generation is similar between the low- and midpenetration cases at low angles. Because the high-penetration case does not share in this similarity, the physics of the high-penetration case maybe different. The directivity of these observations is significant because mixing noise is expected to be most pronounced at sideline (low to mid) angles.

The flowfield details for these cases are discussed in Sec. IV.

B. Spectra Observations

The sound spectra for angles of 60, 90, 110, and 150 deg were studied in detail for all four mixer geometries at the three power settings. The spectra at 90 and 110 deg exhibit some variation in frequency dominance between the high-frequency and low-frequency noise levels depending on which mixer geometry is being used. (The 110-deg spectra are shown in Figs. 12–14.) At these angles, the lobed mixers exhibit the most noise at the high frequencies (3000–12,000 Hz range), whereas the confluent cases show the most noise at the lower frequencies (300–3000 Hz range). The 60-deg spectra (not shown) are similar; however, the spectra of the low-penetration mixer closely mimic those of the confluent case for the low- and midpower settings. The 150-deg spectra (not shown) are dominated by low-frequency noise; however, this effect is reduced greatly with increases in mixer penetration. In general, increased mixer penetration tends to increase noise at low (sideline) angles and high frequencies, but reduces noise at high (downstream) angles.

Because of the local OASPL peak at 110 deg (as shown in Fig. 11 for the midpenetration case at the high-power setting), the 110-deg spectra was of special interest. In Fig. 14 (high-power setting 110-deg spectra), the medium-penetration spectrum peaks well above the high-penetration case with a distinct hump at about 10,000 Hz. The low-penetration spectrum likewise has a distinct hump near 10,000 Hz and is contoured very similar to the midpenetration case. This supports the earlier OASPL observation that there is a significant physical difference between how the high-penetration case and the other lobed mixers create noise. It also suggests that this difference in physical behavior has the effect of limiting the mixing noise increase associated with the high-penetration mixer. A similar midpenetration peak is also present for the midpower setting (Shown in Fig. 13); however, it is less pronounced. The low-power setting spectra, as shown in Fig. 12 does not show this effect. How this behavior may be correlated to the flowfields is discussed in Sec. IV.

Note that not all of the frequencies are of equal importance. The important quantity is the tone-corrected perceived noise level L_{TPN}, which is the measure used in determining aircraft noise ratings.[22] In terms of annoyance, full-scale frequencies between 1500 and 5000 Hz tend to be the worst for humans[21] with 3000 Hz being identified as the most annoying frequency.[23] All of the experimental results in this paper were performed at one-quarter-scale; therefore,

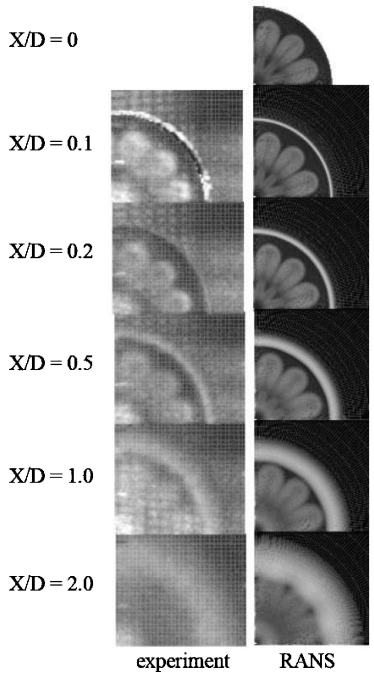

Fig. 15 Low-penetration mixer: square root of TKE from PIV experiment (left) and RANS solution (right).

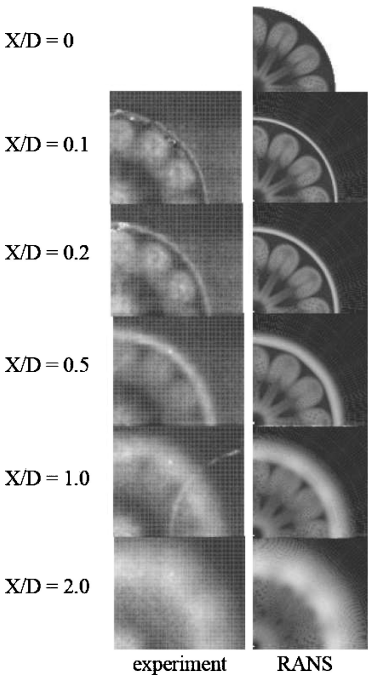

Fig. 16 Mid-penetration mixer: square root of TKE for PIV experiment (left) and RANS solution (right).

the frequencies need to be divided by four to correspond to the full scale. This makes the one-quarter-scale medium-penetration peak at 10,000 Hz for the high-power setting very significant in terms of annoyance for the full-scale case. In general, the confluent and low-penetration mixers produce less noise in the most annoying frequency ranges; however, they have much higher noise levels in the low frequencies. They may also be less efficient in producing thrust due to poorer mixing. (The experiments did not include thrust measurements.) A loss in available thrust would necessitate a higher throttle setting producing an increase in noise and a likely decrease in fuel economy.

IV. Effect of Penetration on the Flowfield

Once the CFD software and numerical scheme were chosen, RANS calculations were made for the four mixer configurations and three power settings at the same conditions in which the jet acoustic tests were run.[24] The computational grid was created at one-quarter scale for consistency with the acoustic test rig, which was also at one-quarter scale. We also had some experimental particle image velocimetry (PIV) data available for these cases. The experimental data available (at the time we did the comparisons with the CFD results) were the axial velocity and the square root of turbulent kinetic energy for the high-power setting only. All of the experimental data were taken at the NASA GRC AAPL.[24,§]

The general procedure was to study the computational and experimental flowfields noting behavior and trends that appear to correspond to the behavior and trends of the sound field. Any observations involving the experimental flowfields were of interest; however, only those that could also be observed in the computed flowfields were considered potentially useful from a design standpoint.

The area within two nozzle diameters downstream of the nozzle exit was the most heavily studied. Within this area were five experimental measurement stations located at 0.1, 0.2, 0.5, 1.0, and 2.0 nozzle diameters downstream of the nozzle exit (Figs. 15–17 top to bottom). Figures 15–17 show the experimental and RANS computed square root of turbulent kinetic energy at these cross sections for the low-, medium-, and high-penetration cases at the high-power setting with a freestream (coflow) Mach number of 0.2. Figures 15–17 also show a RANS computed cross section at the nozzle exit.

The qualitative comparison between the PIV data and the CFD results is quite good, with some differences to be noted. Figures 15–17 show that the vortex size, location, and turbulent kinetic energy

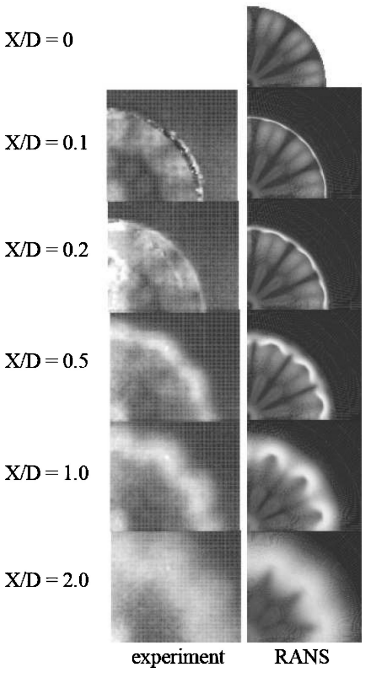

Fig. 17 High-penetration mixer: square root of TKE for PIV experiment (left) and RANS solution (right).

(TKE) levels are comparable. The outside free shear layer of the jet also compares well. The PIV results do, however, show significant TKE levels in the areas away from the major vortex and shear layer, whereas the RANS solutions show near-zero TKE in regions not occupied by these structures. At least part of this discrepancy can be attributed to low levels of freestream turbulence at the solution domain inflows in the CFD. It could also be indicative of the turbulence model's inability to predict turbulence properly in areas with low mean strain rates or within the separated flow region aft of the center cone (Fig. 1).

This low turbulence in certain regions is also demonstrated in Figs. 18–20, where the azimuthally averaged square root of TKE is plotted for cross sections of 0.1, 1.0, and 2.0 nozzle diameters downstream of the nozzle exit for the high-penetration, high-power setting case. In Figs. 18–20, the qualitative nature of the averaged TKE is captured, but once again the computed levels of TKE are low within the core of the jet and in the freestream regions. There is also a large TKE spike at the 0.1 location. This spike is most likely due to the high shear rate associated with the nozzle lip boundary

[§]Data shown here were obtained from private communications with J. Bridges, NASA John H. Glenn Research Center at Lewis Field in June 2003.

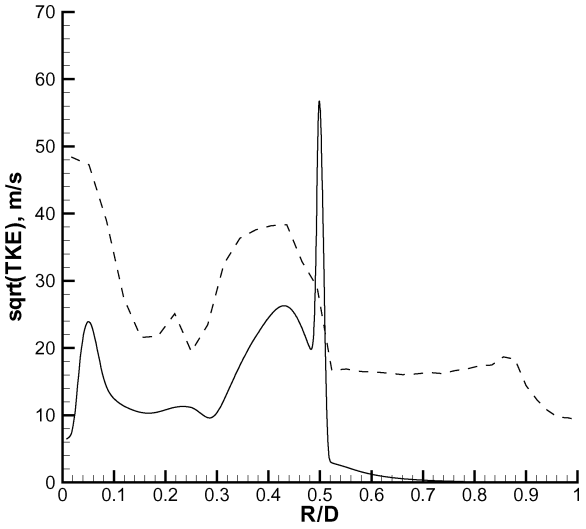

Fig. 18 Azimuthally averaged square root of TKE for high-penetration, high-power setting case at 0.1 nozzle diameters downstreams of the nozzle exit: – – –, PIV data and ——, RANS computed data.

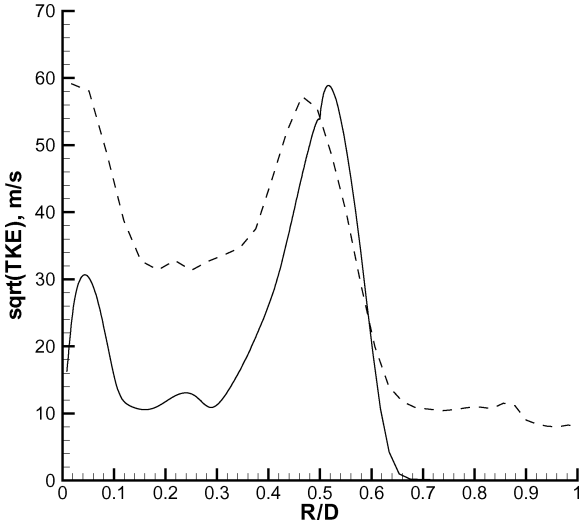

Fig. 19 Azimuthally averaged square root of TKE for high-penetration, high-power setting case at 1.0 nozzle diameters downstreams of nozzle exit: – – –, PIV data and ——, RANS computed data.

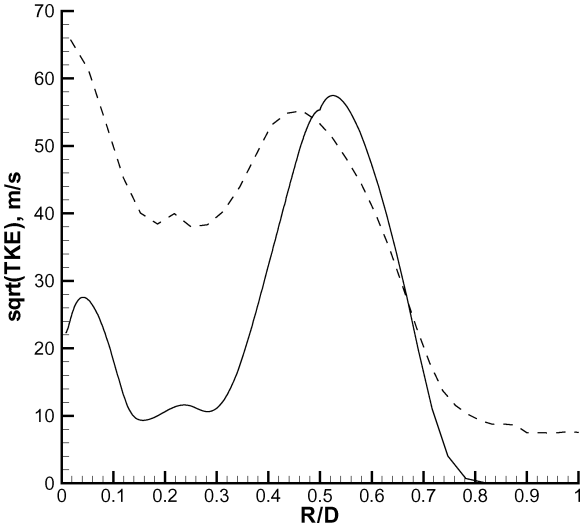

Fig. 20 Azimuthally averaged square root of TKE for high-penetration, high-power setting case at 2.0 nozzle diameters downstreams of nozzle exit: – – –, PIV data and ——, RANS computed data.

layer. It is also possible that the coarseness of the PIV measurement may have caused this feature to be missed in the experimental results.

The mid- and low-power setting flowfields were also computed and were found to be qualitatively almost identical to the high-power setting TKE results, but at a lower overall magnitude. Because of their similarity they are not shown. More detailed results are also available.[25] The confluent flowfield is also not shown because it is axisymmetric and, therefore, relatively simple in terms of flow structure.

A. Flowfield Observations

One of the first things noticed about both the experimental and the CFD results was that the high-penetration flowfields have an immediate interaction at the exit plane between the streamwise vortices and the free shear layer of the jet. There are also similar interactions within the nozzle between the streamwise vortices and the nozzle wall boundary layer. The TKE is high in this near-wall vortex region for the high-penetration cases at the nozzle exit (first cross section), as shown in Fig. 17.

Figure 21 also demonstrates the vortex/wall interaction by showing the vorticity magnitude at the nozzle exit for the high-penetration case at the high-power setting. Figure 21 shows one "pie slice" instead of the full circular cross section. The vorticity is at its highest intensity where the vortex and the wall boundary layer meet, and there is an area of high vorticity that appears as though it is being rolled off the wall and pulled into the vortex. Note that the vortices of the midpenetration case are stronger (higher vorticity magnitude) and more concentrated (smaller and less distorted) than the high-penetration case. This is most likely due in part to energy having been dissipated in the boundary layer as the vortex "scrubs" the nozzle wall. This dissipation near the nozzle exit allows for strong mixing within the nozzle before the vortex contacts the wall, while producing a weakened vortex downstream of the dissipation (outside of the nozzle).

In contrast to the high-penetration flowfields, the vortices and the nozzle wall boundary layer (or free shear layer if outside the nozzle) for the low- and medium-penetration cases are relatively undisturbed by one another near the nozzle exit. This is demonstrated in terms of the square root of TKE for Figs. 15 and 16. In all of these cases, the streamwise vortex structure and the outermost free shear layer of the jet do not substantially interact until 1.0–2.0 nozzle diameters downstream of the nozzle exit.

The final quantity studied in detail was the Mach number. Because this engine uses a converging nozzle, supersonic flow was

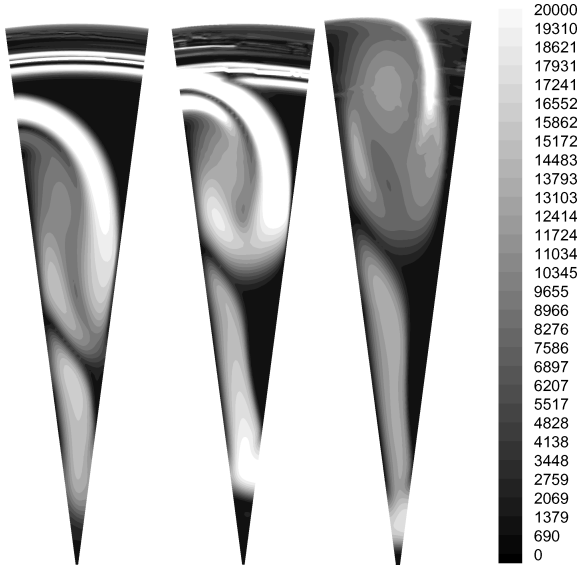

Fig. 21 Vorticity magnitude at exit plane for low- (left), medium- (middle), and high- (right) penetration cases at high-power setting.

not expected, and in a quasi-one-dimensional analysis, it is not even possible. However, because of the three-dimensional nature of real flows, supersonic regions can form as a converging nozzle approaches the choked condition where the nozzle exit is nominally at or near Mach 1.0. The CFD analysis predicts that supersonic flow regions are present at the high-power setting for all of the mixer geometries and at the middle-power setting for all the mixers except the high-penetration case.

As shown in Fig. 22, which shows the Mach contours near the nozzle exit for all four mixer geometries at the high-power setting, shock waves are present inside the lip of the nozzle exit. As shown by Fig. 22, the medium-penetration case at the high-power setting exhibits a significantly larger supersonic region than the other cases. This is believed to be due to the location of the high-velocity and high-temperature flow in the vortex region. Right at the nozzle exit, the nozzle wall turns away from the flow and causes the flow to accelerate more than it would from the contraction alone. This creates a local velocity peak near the lip of the nozzle exit. This local velocity peak is present for all of the mixer configurations and can be seen in Fig. 23, which shows the velocity magnitude contours for all of the mixers at the high-power setting. It is at this local velocity peak that every case has its peak Mach number.

The high-penetration case has the vortex actually contacting the wall and has a very high velocity in this region, but hot flow (increasing the speed of sound) from the vortex is channeled into this region causing its Mach number to be the lowest. Figure 24 (temperature contours near the nozzle exit) shows that the high-penetration case is the only configuration that has hot flow in this region near the nozzle lip. The medium-penetration case does not have as high a velocity in this region as the high-penetration case, but the temperature is lower, because the hot vortex flow is some distance away from the nozzle lip. This lower temperature gives the medium-penetration case the highest peak Mach number and the largest supersonic region even though the velocity near the nozzle lip is lower than for the high-penetration case. The low-penetration and confluent cases

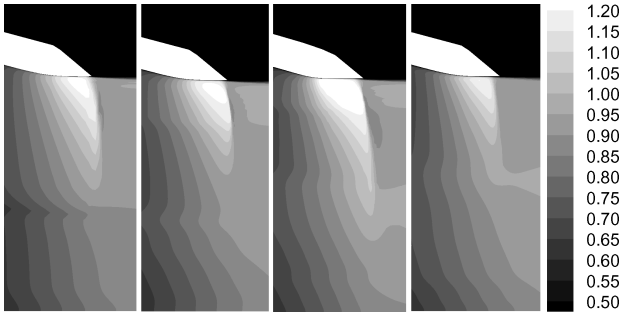

Fig. 22 High-power-setting Mach number contours near nozzle exit for a) confuent, b) low-penetration, c) midpenetration, and d) high-penetration cases.

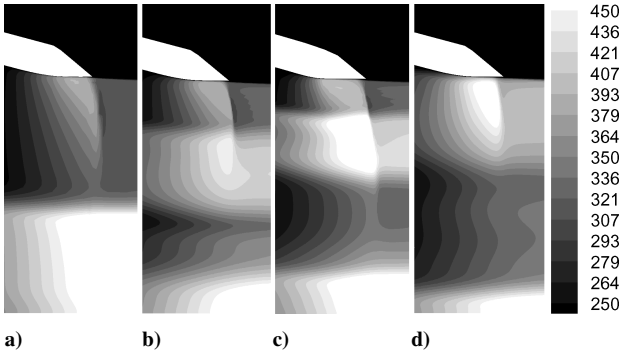

Fig. 23 High-power-setting velocity (meters per second) contours near nozzle exit for a) confuent, b) low-penetration, c) midpenetration, and d) high-penetration cases.

Table 2 Peak Mach numbers for all runs

Setting	Confluent	Low penetration	Midpenetration	High penetration
Low	0.82	0.83	0.87	0.80
Middle	1.05	1.07	1.23	0.97
High	1.23	1.23	1.29	1.21

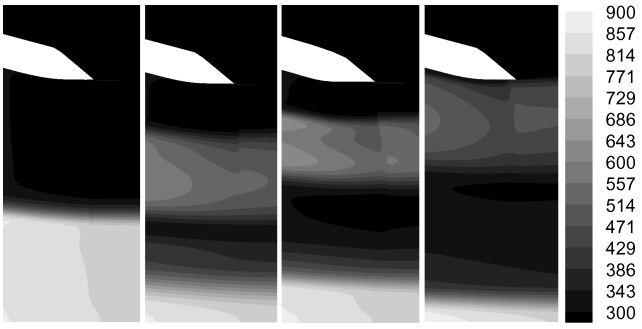

Fig. 24 High-power-setting temperature (Kelvin) contours near nozzle exit for a) confuent, b) low-penetration, c) midpenetration, and d) high-penetration cases.

have temperatures similar to the midpenetration case near the nozzle exit lip; however, they have lower velocities in this region. This causes them to have lower Mach numbers than the midpenetration cases but higher Mach numbers than the high-penetration cases.

The peak Mach numbers for all of the runs are listed in Table 2. As shown in Table 2, the high-penetration cases consistently have the lowest peak Mach numbers, whereas the other cases all show a trend of an increase in Mach number with increased penetration.

B. Relevance to Acoustic Field

As mentioned in the preceding subsection, the streamwise vortices of the high-penetration cases appear to have been weakened through dissipation at the nozzle wall. This point is very important because it has the effect of weakening the vortices as they move into a region suspected as the source of much of the mixing noise. Saiyed et al.[15] denoted this region just outside of the nozzle as the "residual mixing region." They found that this region, where the mixing continues outside of the nozzle, extends at least 1–1.5 nozzle diameters from the nozzle exit and that the mixing noise primarily comes from this external region and not from inside the nozzle.

Assuming that the higher frequencies do primarily emanate from the near downstream region, and given the observations made regarding the unique aspects of the high-penetration sound field and flowfield, one speculative conclusion can be drawn. This is that the interaction of the streamwise vortices with the inside nozzle wall has a beneficial effect in terms of limiting the maximum mixing noise without limiting the benefit of reduced high-angle jet noise. This appears to be partially due to the dissipation of the vortices against the nozzle wall for the high-penetration case; however, this does not explain why the benefit is increased for the higher power settings.

A factor likely affecting the noise generation characteristics of the jet that does depend on the power setting is the presence of supersonic flow. As discussed with the flowfield observations, this supersonic flow is weakest for the high-penetration mixer (where it only exists for the high-power setting) and is strongest for the midpenetration mixer. With reference to Fig. 14, this strong supersonic flow for the midpenetration case coincides with a significant noise peak for the high-power setting at 110 deg and about 10,000 Hz. A much less prominent peak is also present for the midpower setting, and for the low-power setting the effect is gone. The reason for the lower Mach numbers in the high-penetration flow is the location of the streamwise vortices, which convect hot exhaust from the engine core near the nozzle lip where the highest Mach numbers occur. This hot flow and the corresponding lower Mach number could certainly

be a contributing factor in limiting the high-frequency (mixing) noise of the high-penetration case at high-power settings and sideline angles, and it explains the dependence on the power setting. Tester et al.[9] have also recognized an increase in noise in the high frequencies that could be attributed to supersonic flow and have referred to it as "high Mach number lift." Unfortunately, without a more complete set of subsonic flowfield and noise data, it is difficult to differentiate between the high Mach number effects and the effects attributable to vortex/wall interactions. Moreover, these flow phenomena are closely coupled because the location of the vortex has a strong effect on both the velocity and temperature distributions near the nozzle exit.

V. Conclusions

We used the WIND CFD code and Menter's SST turbulence model to compute the RANS flowfields of different internal mixer designs. These flowfields were then examined along with experimental noise data collected at the NASA GRC AAPL.[20] Four different mixer geometries at three different power settings were selected for this project. The variation in mixer geometry was limited to a single parameter, the mixer penetration height. The four different geometries, referred to as high penetration, medium penetration, low penetration, and confluent (no penetration), exhibited significant variation in their acoustic performance.

It was found that the noise at angles of less than 120 deg (measured from the upstream jet axis) is such that the high-penetration mixer produces about the same OASPL at sideline and low (upstream) angles as the midpenetration mixer for medium- and high-throttle settings. However, under these same conditions, the high-penetration mixer exhibits a lower increase in OASPL (compared to the coflow mixer) for angles above 120 deg. Because of this, there is some overall benefit in reducing noise by increasing the mixer penetration from the midpenetration geometry to the high penetration.

The flowfield produced by the high-penetration mixer configuration is quite different in detail from those produced by the low- and medium-penetration mixers. Whereas the low- and medium-penetration mixers have separate streamwise vortices and free shear layers, the high-penetration flowfield exhibits an immediate interaction and rapid merging of these distinctly different flow structures at the nozzle exit plane. There is also considerable interaction between the vortices and the boundary layer inside the nozzle. We can argue that the streamwise vortices scrubbing the nozzle wall limits the amount of low-angle (mixing) noise being produced. This is partially due to the increased dissipation of the vortex near the nozzle wall. This has the effect of weakening the vortex just before it exits the nozzle, thus, allowing for strong vortex mixing within the nozzle and weaker mixing mechanism noise outside of the nozzle.

Another factor likely influencing the acoustic behavior is the presence of supersonic flow near the nozzle exit for all of the high-power setting cases and all of the midpower setting cases except for the high-penetration case. For all cases, the high-penetration mixer produced the lowest peak Mach numbers. As with the scrubbing, this is due to the location of the vortices near the nozzle wall. For the high-penetration case, these vortices convect hot flow into the supersonic regions, thus, raising the speed of sound and lowering the peak Mach number. It is believed that the supersonic flow contributes significantly to the high-frequency portion of the sideline noise at the higher power settings. It is, however, difficult to differentiate between the high Mach number effects and the vortex/wall interaction effects.

Acknowledgments

This project was a joint effort with Rolls–Royce, Indianapolis, and was sponsored by the Indiana 21st Century Research and Technology Fund. The first author was supported by a Department of Education Graduate Assistance in Areas of National Need fellowship. Loren Garrison from Purdue University and Shyam Neerarambam from Rolls–Royce, Indianapolis provided helpful discussions and technical assistance with WIND. All WIND calculations were performed on the 104-processor School of Aeronautics and Astronautics LINUX cluster acquired by a Defense University Research Instrumentation Program grant sponsored by Army Research Office, and all of the acoustic experiments were made available by Bill Dalton of Rolls–Royce and James Bridges of NASA John H. Glenn Research Center at Lewis Field. The first author is also indebted to his former colleague Ali Uzun for lending his expertise in technical matters.

References

[1]Freund, J. B., "Noise Sources in a Low Reynolds Number Turbulent Jet at Mach 0.9," *Jounal of Fluid Mechanics*, Vol. 438, 2001, pp. 277–305.

[2]Uzun, A., Blaisdell, G. A., and Lyrintzis, A. S., "Application of Compact Schemes to Large Eddy Simulations of Turbulent Jets," *Journal of Scientific Computing*, Vol. 21, No. 3, 2004, pp. 283–319.

[3]Bogey, C., Bailly, C., and Juve, D., "Noise Investigation of a High Subsonic, Moderate Reynolds Number Jet Using a Compressible Large Eddy Simulation," *Theoretical and Computational Fluid Dynamics*, Vol. 16, No. 4, 2003, pp. 273–297.

[4]Mani, R., Balsa, T. F., and Gliebe, P. R., "High Velocity Jet Noise Source Location and Reduction: Task 2-Theoretical Developments and Basic Experiments," Federal Aviation Administration, Rept. FAA-RD-76-79-II, May 1978.

[5]Lighthill, M. J., "On Sound Generated Aerodynamically: I. General Theory," *Proceedings of the Royal Society of London, Series A: Mathematical and Physical Sciences*, Vol. 211, No. 1107, 1952, pp. 564–587.

[6]Barber, T. J., and Chiappetta, L. M., "An Assessment of Jet Noise Analysis Codes for Multistream Axisymmetric and Forced Mixer Nozzles," AIAA Paper 96-0750, Jan. 1996.

[7]Fisher, M. J., Preston, G. A., and Bryce, W. D., "A Modelling of the Noise for Simple Coaxial Jets, Part I: With Unheated Primary Flow," *Journal of Sound and Vibration*, Vol. 209, No. 3, 1998, pp. 385–403.

[8]Fisher, M. J., Preston, G. A., and Bryce, W. D., "A Modelling of the Noise for Simple Coaxial Jets, Part II: With Heated Primary Flow," *Journal of Sound and Vibration*, Vol. 209, No. 3, 1998, pp. 405–417.

[9]Tester, B. J., Fisher, M. J., and Dalton, W. N., AIAA Paper 2004-2897, May 2004.

[10]Tester, B. J., and Fisher, M. J., "A Contribution to the Understanding and Prediction of Jet Noise Generation in Forced Mixers, Part II: Flight Effects," AIAA Paper 2005-3094, May 2005.

[11]Garrison, L. A., Dalton, W. N., Lyrintzis, A. S., and Blaisdell, G. A., "Investigation of Extensions of the Four-Source Method for Predicting Forced Mixer Jet Noise," AIAA Paper 2003-3165, May 2003.

[12]Garrison, L. A., Dalton, W. N., Lyrintzis, A. S., and Blaisdell, G. A., "Semi-Empirical Noise Models for Predicting the Noise from Jets with Interal Forced Mixers," *International Journal of Aeroacoustics*, Vol. 5, No. 2, 2006 (in press).

[13]Garrison, L. A., Lyrintzis, A. S., Blaisdell, G. A., and Dalton, W. N., "Computational Fluid Dynamics Analysis of Flows with Internal Forced Mixers," AIAA Paper 2005-2887, May 2005.

[14]Pinker, R. A., and Strange, P. J. R., "The Noise Benefits of Forced Mixing," AIAA Paper 98-2256, June 1998.

[15]Saiyed, N. H., Bridges, J. E., and Krejsa, E. A., "Core and Fan Streams' Mixing Noise Outside the Nozzle for Subsonic Jet Engines with Internal Mixers," AIAA Paper 96-1667, May 1996.

[16]Wright, C. W., Blaisdell, G. A., and Lyrintzis, A. S., "Using RANS to Predict the Performance of Mixers in Reducing Jet Noise," AIAA Paper, 2004-1274, Jan. 2004.

[17]"WIND User's Guide," NPARC Alliance, NASA John H. Glenn Research Center, at Lewis Field, OH, May 2002.

[18]Spalart, P. R., and Allmaras, S. R., "A One-Equation Turbulence Model for Aerodynamic Flows," AIAA Paper 92-0439, Jan. 1992.

[19]Menter, F. R., "Two-Equation Eddy-Viscosity Turbulence Models for Engineering Applications," *AIAA Journal*, Vol. 32, No. 3, 1994, pp. 1598–1605.

[20]Bridges, J. E., "Measurements of the Aeroacoustic Sound Source in Hot Jets," AIAA Paper 2003-3130, May 2003.

[21]Mengle, V. G., Dalton, W. N., Bridges, J. E., and Boyd, K. C., "Noise Reduction with Lobed Mixers: Nozzle-Length and Free-Jet Speed Effects," AIAA Paper 97-1682, May 1997.

[22]Kinsler, L. E., Frey, A. R., Coppens, A. B., and Sanders, J. V., *Fundamentals of Acoustics*, Wiley, New York, 2000, Chap. 12.

[23]Mengle, V. G., "Optimization of Lobe Mixer Geometry and Nozzle Length for Minimum Jet Noise," AIAA Paper 2000-1963, June 2000.

[24]Bridges, J. E., and Wernet, W., "Cross-Stream PIV Measurements of Jets with Internal Lobed Mixers," AIAA Paper 2004-2896, May 2004.

[25]Wright, C. W., "Investigating Correlations Between Rynolds Averaged Flow Fields and Noise for Forced Mixed Jets," M.S. Thesis, School of Aeronautics and Astonautics, Purdue Univ., West Lafayette, IN, May 2004.